

Polarization of the Cosmic Microwave Background from Non-Uniform Reionization

Guo-Chin Liu^{1,2}, Naoshi Sugiyama², Andrew J. Benson^{3,4}, C. G. Lacey⁵ and Adi Nusser⁶

¹Department of Physics, Kyoto University, Kyoto 606-8502, Japan

²Division of Theoretical Astrophysics, National Astronomical Observatory Japan, Mitaka, 181-8588, Japan

³California Institute of Technology, MC 105-24, Pasadena, CA 91125, U.S.A.

⁴Department of Physics, University of Durham, UK

⁵SISSA, via Beirut 2-4, 34014 Trieste, Italy

⁶The Physics Department, The Technion-Israel Institute of Technology, Technion City, Haifa 32000, Israel

ABSTRACT

We study the signal in the Cosmic Microwave Background (CMB) polarization anisotropy resulting from patchy reionization. It is well known that the primordial polarization of the CMB is very sensitive to the details of reionization. Combining a semi-analytic model of galaxy formation, in which the optical depth to the reionization epoch is in the range 0.014 to 0.048, with a high resolution N-body simulation we find that reionization generates a peak with amplitude $0.05 \sim 0.15 \mu\text{K}$ at large angular scales ($l \sim 3$). The position of this peak reveals the size of the horizon at reionization, whilst its amplitude is a measure of the optical depth to reionization. On small scales ($l \gtrsim 6000$), ionized patches prior to full reionization create a second order polarization signal due to the coupling of the free electron density fluctuation with the quadrupole moment of the temperature anisotropy. Careful study reveals that the coupling generates the same power spectra for electric and magnetic modes, whose amplitudes of polarization anisotropies from this process are predicted to be $\sim 10\text{nK}$. The amplitude depends strongly on the total baryon density Ω_b and on the spatial correlations of the free electron density in the ionized regions, and weakly on the fraction of ionizing photons able to escape their source galaxy, f_{esc} . The first- and second-order signals are therefore sensitive to the details of how the reionization occurred. Detection of these signals will place important constraints on the reionization history of the Universe.

Subject headings: cosmology: theory - - cosmology:cosmic microwave background - - galaxies: formation - - intergalactic medium

1. INTRODUCTION

The secondary anisotropies in the Cosmic Microwave Background (CMB) provide a laboratory for the study of the reionization epoch of the Universe. With the rapid improvement in CMB experimental sensitivity and resolution, it is timely to discuss the signals introduced by the process of reionization, which are at the μK level or below. In this paper, we concentrate on the CMB *polarization* in models with inhomogeneous reionization. It is well known that the primordial polarization is generated by the quadrupole of the temperature anisotropy at the recombination epoch through Thomson scattering. The same mechanism occurs at the reionization epoch and again distorts the shape of the polarization power spectrum. It has been pointed out by Ng & Ng (1996) and Zaldarriaga (1997) that this leads to the polarization anisotropy being suppressed on small scales but enhanced on large scales. The degree of suppression and enhancement typically depend on the optical depth to reionization. Although the polarization anisotropy amplitude is estimated to be much smaller than that in the temperature, it is advantageous to consider the polarization signal since it is generated when photons and electrons scatter for the last time. Thus, unlike the temperature fluctuations which are affected by the gravitational potential between recombination and present, we can find a very clear signal of the last scattering epoch in the polarization angular power spectrum. By using the results from the previous work of Benson et al. (2000; hereafter Paper I), in which the reionization history of the intergalactic medium (IGM) was obtained from a semi-analytic model of galaxy formation, we first investigate the first-order distortion of the polarization anisotropy spectrum.

Although the temperature and polarization anisotropies are small, they are cosmologically interesting, as second order effects arise from the modulation of the number density of free electrons close to the reionization epoch as in the Vishniac effect (Vishniac 1987). Historically, work in this field began by considering the temperature anisotropies, with the fluctuations in the free electron density assumed to follow the density variations of the matter in a homogeneous reionization, the so-called density modulation (Vishniac 1987, Jaffe & Kamionkowski 1998). However, any realistic model of how this reionization might have taken place is thought to be patchy or inhomogeneous. Shapiro & Giroux (1987) and Sato (1994) investigated the evolution of the ionization front with the analytic method. Recent numerical simulations of radiative hydrodynamics also reveal the patchiness of the reionization (Gnedin 2000). Gruzinov & Hu (1998) introduced a toy model in which the universe is reionized in *uncorrelated* spherical patches. More realistic methods such as full simulations (Gnedin & Jaffe 2000) or semi-analytic models for the secondary effects have also been studied by a number of authors (Springel, White, & Hernquist 2000, Bruscoli et al. 2000, Paper I, Valageas, Balbi, & Silk 2000). So far these works have concluded that second order effects make significant contributions to the temperature anisotropy on small-scales ($l \gtrsim 3000$) and peak in the range $0.1\mu\text{K}$ to $1\mu\text{K}$.

While the second order temperature anisotropies are well studied, those of the polarization anisotropy spectrum have received relatively little attention. Seshadri & Subramanian (1998) and Weller (1999) discussed this effect in density modulation and patchy reionization models,

respectively. Here, we consider second order polarization anisotropies in a more realistic model than has previously been possible. The free electron density fluctuations are taken from our previous work (Paper I), in which we combined a semi-analytic model of galaxy formation with an N-body simulation of the distribution of dark matter in the universe to determine the distribution of ionized regions. In this paper, we consider only the scalar mode for primordial fluctuations. In case of the first order perturbation theory, the scalar mode fluctuations produce only the electric (E-) mode of polarization. For the second order perturbations, however, this may not be the case. Since the polarization anisotropies are induced by the coupling between primordial CMB quadrupole anisotropies and density fluctuations in the ionized medium, axisymmetry is broken and the B-mode is also produced (Hu 2000). Moreover, there is another source of polarization, i.e., the kinetic quadrupole, besides the primordial CMB quadrupole anisotropy. The isotropic CMB gains a quadrupole anisotropy from the quadratic Doppler effect due to the peculiar motion of the ionized medium (Sunyaev & Zel'dovich 1980). This kinetic quadrupole can generate the magnetic (B-) mode as well as the electric mode. However, the amplitude of the polarization generated by this kinetic quadrupole contribution is much smaller than the one generated by the coupling between the primordial CMB quadrupole anisotropies and the inhomogeneous distribution of the ionized medium (Hu 2000).

This paper is organized as follows. In §2, we present the Boltzmann equation for the first and second order polarization anisotropies. We then derive the E- and B-mode power spectra by use of the Boltzmann equation. In §3, we give a brief overview of our model for inhomogeneous reionization and show our numerical results for both the first and second order polarization spectrum. §4 is devoted to our conclusions. Throughout this paper we work in units where $c = 1$.

2. SECOND ORDER EFFECTS FROM THE REIONIZATION EPOCH

2.1. Boltzmann Equation and Second Order Polarization

The evolution of the temperature perturbation, $\Delta_T(\mathbf{x}, \hat{\mathbf{n}}, \tau)$, and the polarization perturbation, $\Delta_P(\mathbf{x}, \hat{\mathbf{n}}, \tau)$, are governed by the Boltzmann equation (Bond & Efstathiou 1984, Ma & Bertschinger 1995, Peebles & Yu 1970). Here \mathbf{x} is the comoving coordinate, $\tau \equiv \int dt/a$ the conformal time, where a is the expansion factor normalized to unity today, and $\hat{\mathbf{n}}$ the direction of photon propagation. Following Zaldarriaga & Seljak (1997), to calculate the polarization perturbation Δ_P we work in terms of the perturbed Stokes parameters $\Delta_{Q\pm iU}$ (see §2.2). In this paper, we do not include tensor perturbations, and derive the Boltzmann equation in the conformal Newtonian gauge. Readers interested in the synchronous gauge or the transformation between these two gauges are referred to Ma & Bertschinger (1995). In the Newtonian gauge, the perturbations are specified by two scalar potentials, ϕ and ψ , which play the role of the gravitational potential and the fractional perturbation to the spatial curvature, respectively. The Boltzmann equation then

states that

$$\dot{\Delta}_T + \hat{\mathbf{n}}_i \partial_i \Delta_T = \dot{\phi} - \hat{\mathbf{n}}_i \partial_i \psi + n_e \sigma_T a(\tau) \left(-\Delta_T + \Delta_{T0} + \hat{\mathbf{n}}_i v_{bi} - \frac{\sqrt{5}\pi}{5} \sum_{m=-2}^{m=2} Y_2^m(\hat{\mathbf{n}}) \Pi^{(m)} \right), \quad (1)$$

$$\dot{\Delta}_{Q\pm iU} + \hat{\mathbf{n}}_i \partial_i \Delta_{Q\pm iU} = n_e \sigma_T a(\tau) \left(-\Delta_{Q\pm iU} + \sqrt{\frac{6\pi}{5}} \sum_{m=-2}^{m=2} \pm 2 Y_2^m(\hat{\mathbf{n}}) \Pi^{(m)} \right), \quad (2)$$

where ${}_s Y_l^m$ is spherical harmonics with spin-weight s , $\Pi^{(m)}$ is defined in terms of the quadrupole components of the temperature and polarization perturbations as

$$\Pi^{(m)}(\mathbf{x}, \tau) \equiv \Delta_{T2}^{(m)}(\mathbf{x}, \tau) + 12\sqrt{6}\Delta_{+,2}^{(m)}(\mathbf{x}, \tau) + 12\sqrt{6}\Delta_{-,2}^{(m)}(\mathbf{x}, \tau). \quad (3)$$

Here the derivatives are taken with respect to the conformal time, v_b is the velocity of baryons, n_e is the free electron number density, and σ_T is the Thomson cross section. We have also expanded the perturbations in the radiation field in spherical harmonics ${}_s Y_m^m$ with appropriate spin weight s (see also §2.2)

$$\begin{aligned} \Delta_T(\mathbf{x}, \hat{\mathbf{n}}, \tau) &= \sum_{lm} (-i)^l \sqrt{4\pi(2l+1)} \Delta_{Tl}^{(m)}(\mathbf{x}, \tau) Y_l^m(\hat{\mathbf{n}}), \\ \Delta_{Q\pm iU}(\mathbf{x}, \hat{\mathbf{n}}, \tau) &= \sum_{lm} (-i)^l \sqrt{4\pi(2l+1)} \Delta_{\pm,l}^{(m)}(\mathbf{x}, \tau) {}_2 Y_l^m(\hat{\mathbf{n}}). \end{aligned} \quad (4)$$

When we calculate the perturbations for a mode with wavenumber \mathbf{k} , we define the Y_l^m 's in a coordinate system for which the z -axis is parallel to \mathbf{k} . To calculate the first order effect for scalar modes, we can set $m = 0$, as in Zaldarriaga & Seljak (1997), due to the axisymmetry of the radiation field around the mode axis for this case. However, their expansion is not valid for studying the second order effect, in which the rotational symmetry around the wavevector is broken by coupling to other modes. It is very important to take into account $m \neq 0$ modes for the calculating the second order effect, otherwise the (artificially imposed) axisymmetry guarantees that no magnetic mode can be generated. This is why Weller (1999), who assumed axial symmetry following Seshadri & Subramanian (1998), obtained only the electric mode of polarization for the second order effect. As was found by Hu (2000), who employed the weak-coupling approximation, the magnetic mode of polarization is also generated in the case of the second order effect. Thus, the expansion in equation (4) is more general and useful for our calculation.

On small scales, as pointed out by Kaiser (1984), the contribution to secondary temperature anisotropies from homogeneous reionization tends to cancel along the line of sight. Thus, the first order effect on the temperature and polarization anisotropies from the reionization epoch is suppressed at small angles. Hereafter, we concentrate on polarization and develop an equation for the visibility-modulated effect which is the dominant source on small scales.

Firstly, we write the inhomogeneous distribution of the free electron number density as

$$n_e(\mathbf{x}, \tau) = \bar{n}_e(\tau)[1 + \delta_e(\mathbf{x}, \tau)], \quad (5)$$

where δ_e is the fluctuation of electron number density and $\bar{}$ denotes the background quantity. Then, equation (2) can be rewritten in terms of Fourier modes as follows,

$$\begin{aligned} \dot{\Delta}_{Q_{\pm iU}}(\mathbf{k}, \tau) + ik\mu\Delta_{Q_{\pm iU}}(\mathbf{k}, \tau) &= \bar{n}_e\sigma_T a(\tau) \left(-\Delta_{Q_{\pm iU}}(\mathbf{k}, \tau) - R_{\pm}(\mathbf{k}, \tau) \right. \\ &\quad \left. \sum_m \sqrt{\frac{6\pi}{5}} {}_{\pm 2}Y_2^m(\hat{\mathbf{n}}) \left(\Pi^{(m)}(\mathbf{k}, \tau) + S^{(m)}(\mathbf{k}, \tau) \right) \right), \end{aligned} \quad (6)$$

where $S^{(m)}(\mathbf{k}, \tau)$ and $R_{\pm}(\mathbf{k}, \tau)$ are the Fourier modes of the coupling of $\delta_e(\mathbf{x}, \tau)$ to $\Pi^{(m)}(\mathbf{x}, \tau)$ and $\Delta_{Q_{\pm iU}}(\mathbf{x}, \tau)$, respectively. In other words,

$$S^m(\mathbf{k}, \tau) = \int d^3\mathbf{p} \delta_e(\mathbf{k} - \mathbf{p}, \tau) \Pi^{(m)}(\mathbf{p}, \tau), \quad (7)$$

$$R_{\pm}(\mathbf{k}, \tau) = \int d^3\mathbf{p} \delta_e(\mathbf{k} - \mathbf{p}, \tau) \Delta_{Q_{\pm iU}}(\mathbf{p}, \tau). \quad (8)$$

The polarization perturbations at the present time can be obtained by integrating the Boltzmann equation (6) along the line of sight (Zaldarriaga & Seljak 1997)

$$\begin{aligned} \Delta_{Q_{\pm iU}}(\mathbf{k}, \mu, \tau_0) &= \int_0^{\tau_0} d\tau e^{ik(\tau_0 - \tau)\mu} g(\tau) \\ &\times \left(\sqrt{\frac{6\pi}{5}} \sum_m {}_{\pm 2}Y_2^m(\hat{\mathbf{n}}) \left[\Pi^{(m)}(\mathbf{k}, \tau) + S^{(m)}(\mathbf{k}, \tau) \right] - R_{\pm}(\mathbf{k}, \tau) \right), \end{aligned} \quad (9)$$

where $\mu = \mathbf{k} \cdot \hat{\mathbf{n}}$, and $g(\tau)$ is the visibility function defined as

$$g(\tau) \equiv -\frac{d\kappa}{d\tau} e^{\kappa(\tau_0) - \kappa(\tau)}, \quad (10)$$

with $\kappa(\tau) \equiv -\int_{\tau}^{\tau_0} d\tau' a n_e \sigma_T$. The visibility function has a simple physical meaning, being the probability that a photon scattered at epoch τ reaches the observer at the present time, τ_0 . Equation (9) can then be given a simple interpretation, since $\Pi^{(m)}(\mathbf{k}, \tau)$ acts as a first order source term while $R_{\pm}(\mathbf{k})$ and $S^{(m)}(\mathbf{k})$ are the contributions from the second order effect. To simplify the calculation, we neglect $R_{\pm}(\mathbf{k})$ and $\Delta_{\pm, 2}^{(m)}$ in $S^{(m)}(\mathbf{k})$ because the temperature perturbations typically dominate over the polarization perturbations. Furthermore, we assume the first order temperature quadrupole $\Delta_{T2}^{(m)}$ is *uncorrelated* with δ_e due to the fact that the dominant contributions to these come from large and small scales, respectively. That is, we regard the source term for the second order polarization as

$$\begin{aligned} S^{(m)}(\mathbf{k}, \tau) &\simeq \delta_e(\mathbf{k}, \tau) \int d^3\mathbf{p} \Delta_{T2}^{(m)}(\mathbf{p}, \tau) \\ &\equiv \delta_e(\mathbf{k}, \tau) Q_2^{(m)}(\tau), \end{aligned} \quad (11)$$

with $Q_2^{(m)}(\tau)$ defined as $Q_2^{(m)}(\tau) \equiv \int d^3\mathbf{p} \Delta_{T2}^{(m)}(\mathbf{p}, \tau)$ for convenience. Recall the scalar mode in linear theory only generates $m = 0$ component in the \mathbf{p} -basis, i.e., $\Delta_{T2}^{(0)} Y_2^0(\beta, \alpha)$ where β and α

are the polar and azimuthal angles defining $\hat{\mathbf{n}}$ in this basis. Using the addition theorem, we can project the component in the \mathbf{p} -basis onto the \mathbf{k} - basis (see Ng & Liu 1999),

$$\sum_m Y_l^{m*}(\hat{\mathbf{n}})Y_l^m(\hat{\mathbf{p}}) = \sqrt{\frac{2l+1}{4\pi}}Y_l^0(\beta, \alpha), \quad (12)$$

It then follows that

$$Q^{(m)} = \sqrt{\frac{4\pi}{5}} \int d^3\mathbf{p} \Delta_{T_2}^{(0)}(\mathbf{p}) Y_2^{m*}(\hat{\mathbf{p}}). \quad (13)$$

Finally, the solution of $\Delta_{Q\pm iU}$ becomes

$$\Delta_{Q\pm iU}(\mathbf{k}, \hat{\mathbf{n}}, \tau_0) = \sqrt{\frac{6\pi}{5}} \int_0^{\tau_0} d\tau e^{ik(\tau_0-\tau)\mu} g(\tau) \sum_m \pm 2 Y_2^m(\hat{\mathbf{n}}) X^{(m)}(\mathbf{k}, \tau), \quad (14)$$

where $X^{(m)}(\mathbf{k}, \tau)$ equals $\Pi^{(0)}(\mathbf{k}, \tau)$ or $S^{(m)}(\mathbf{k}, \tau)$ for the first and second order signals, respectively.

2.2. Stokes Parameters and the Power Spectrum

We follow the approach of Zaldarriaga & Seljak (1997) of calculating the polarization in terms of the electric and magnetic modes. We start with the description of the polarization perturbation in terms of the Stokes parameters Q and U . If we consider a wave traveling in the \hat{z} direction, Q is the difference in intensity polarized in the \hat{y} and \hat{x} directions, while U is the difference in the $(\hat{x} + \hat{y})/\sqrt{2}$ and $(\hat{x} - \hat{y})/\sqrt{2}$ directions. The circular polarization parameter, V , cannot be produced by scattering, so we will not mention it further. Polarization is more complicated than temperature because it depends on the choice of coordinates. Under a right-hand rotation through an angle ϕ around the \hat{z} axis the temperature is invariant, while Q and U are transformed to

$$(Q \pm iU)'(\hat{\mathbf{n}}) = e^{\mp 2i\phi} (Q \pm iU)(\hat{\mathbf{n}}). \quad (15)$$

Thus the functions $Q \pm iU$ have spin ± 2 , and should be expanded in spherical harmonics of spin ± 2 .

It is possible to produce a rotationally invariant polarization field if we introduce the spin raising and lowering operators ∂ and $\bar{\partial}$ (Newman & Penrose 1966)

$$\begin{aligned} \partial\eta &= -(\sin\theta)^s \left[\frac{\partial}{\partial\theta} + i \csc\theta \frac{\partial}{\partial\phi} \right] (\sin\theta)^{-s} \eta, \\ \bar{\partial}\eta &= -(\sin\theta)^{-s} \left[\frac{\partial}{\partial\theta} - i \csc\theta \frac{\partial}{\partial\phi} \right] (\sin\theta)^s \eta, \end{aligned} \quad (16)$$

with η as a spin- s field. If they act on the spin- s spherical harmonics, we have

$$\begin{aligned} \partial_s Y_{lm} &= [(l-s)(l+s+1)]^{\frac{1}{2}} {}_{s+1}Y_{lm}, \\ \bar{\partial}_s Y_{lm} &= -[(l+s)(l-s+1)]^{\frac{1}{2}} {}_{s-1}Y_{lm}. \end{aligned} \quad (17)$$

The new bases of the rotationally invariant polarization field, called the electric mode and magnetic mode, are defined as

$$\begin{aligned}\Delta_E &\equiv -\frac{1}{2} \left(\bar{\partial}^2 \Delta_{Q+iU} + \partial^2 \Delta_{Q-iU} \right), \\ \Delta_B &\equiv -\frac{i}{2} \left(\bar{\partial}^2 \Delta_{Q+iU} - \partial^2 \Delta_{Q-iU} \right).\end{aligned}\tag{18}$$

The values of Δ_E and Δ_B at a particular direction in the sky are independent of the coordinate system used to define them (unlike Δ_Q and Δ_U). We work in the coordinate system where $\hat{k} \parallel \hat{z}$ and define $Q > 0$ ($Q < 0$) in the direction \hat{e}_θ (\hat{e}_ϕ). For a scalar mode in first-order perturbation theory, the radiation field is axisymmetric around the wavevector. The polarization is produced by scattering of the quadrupolar component of the radiation field, and so has only a Δ_Q component, but no Δ_U component (which would correspond to a polarization angle at 45° to the \hat{e}_θ - \hat{e}_ϕ axes), thus $\Delta_{Q+iU} = \Delta_{Q-iU} = \Delta_Q$. Furthermore, Δ_Q has no ϕ -dependence, so $\bar{\partial}^2 = \partial^2$ (eq. 16). As a consequence, $\Delta_E = -\partial^2 \Delta_Q = -\bar{\partial}^2 \Delta_Q$ and $\Delta_B = 0$. This result is important because it shows that no magnetic mode can be produced by scalar modes (density perturbations) in first order perturbation theory. However, as we will show later, the same situation does not occur in the second order polarization because the coupling between modes breaks axisymmetry.

Again, following Zaldarriaga & Seljak (1997), the power spectra of the electric mode and magnetic mode can be defined as

$$C_{(E,B)l} \equiv \frac{1}{2l+1} \frac{(l-2)!}{(l+2)!} \sum_m \int d^3\mathbf{k} \langle |\Delta_{(E,B)l}^{(m)}(\mathbf{k}, \tau = \tau_0)|^2 \rangle,\tag{19}$$

where $\Delta_{(E,B)l}^{(m)}$ can be extracted using

$$\Delta_{(E,B)l}^{(m)}(\mathbf{k}) = \int d\Omega Y_l^m(\theta, \phi) \Delta_{(E,B)}(\mathbf{k}).\tag{20}$$

To calculate equation (20), we can apply the spin raising and lowering operators (eq. 16 or 17) to the polarization perturbations in equation (14) twice. But the plane wave $e^{ik(\tau_0-\tau)\mu}$ itself carries an angular dependence, thus we expand the plane wave in a series of spherical waves using the Rayleigh equation

$$e^{ik(\tau_0-\tau)\mu} = \sum_l (-i)^l \sqrt{4\pi(2l+1)} j_l[k(\tau_0-\tau)] Y_l^0(\hat{\mathbf{n}}),\tag{21}$$

where $j_l[k(\tau_0-\tau)]$ is the spherical Bessel function. Furthermore, we calculate the product of two spherical harmonics with spin by using the Clebsch-Gordan relation (Sakurai 1985)

$$\begin{aligned}s_1 Y_{l_1}^{m_1} s_2 Y_{l_2}^{m_2} &= \frac{\sqrt{(2l_1+1)(2l_2+1)}}{4\pi} \sum_{lms} \langle l_1, l_2, m_1, m_2 | l, m \rangle \\ &\times \langle l_1, l_2, -s_1, -s_2 | l, -s \rangle \sqrt{\frac{4\pi}{2l+1}} s Y_l^m.\end{aligned}\tag{22}$$

m	$T_{El}^{(m)}$	$T_{Bl}^{(m)}$
0	$(-i)^l \frac{j_l(kr)}{(kr)^2}$	0
± 1	$\mp (-i)^l \frac{1}{(2l+1)kr} \sqrt{\frac{1}{6l(l+1)}} [j_l(kr) - (l+1)j_{l-1}(kr)]$	$\pm \sqrt{\frac{(-i)^l}{6l(l+1)}} \frac{j_l(kr)}{(kr)^2}$
± 2	$\pm \frac{(-i)^l}{2l+1} \sqrt{\frac{(l-2)!}{24(l+2)!}} \left(\left[\frac{(l+2)(l+1)}{2l-1} + \frac{l(l+1)}{2l+3} + 6 \frac{(2l+1)(l-1)(l+2)}{(2l-1)(2l+3)} \right] \right.$ $\left. \times j_l(kr) - (l+2)(l+1) \frac{j_{l-1}(kr)}{kr} + l(l-1) \frac{j_{l+1}(kr)}{kr} \right)$	$\mp \frac{(-i)^l}{2l+1} \sqrt{\frac{(l-2)!}{6(l+2)!}} [(l+2)j_{l-1}(kr)$ $- (l-1)j_{l+1}(kr)]$

Table 1: $T_{(E,B)l}^{(m)}$ in equation (23)

The expression for $\Delta_{(E,B)l}^{(m)}(\mathbf{k}, \tau)$ then becomes

$$\Delta_{(E,B)l}^{(m)}(\mathbf{k}, \tau) = \frac{3}{2} \sqrt{\pi} \frac{(l+2)!}{(l-2)!} \sqrt{2l+1} \int_0^{\tau_0} d\tau g(\tau) X^{(m)}(\mathbf{k}, \tau) T_{(E,B)l}^{(m)}(kr), \quad (23)$$

with $r = \tau_0 - \tau$. In Table 1, we list the results of $T_{(E,B)l}^{(m)}(kr)$, in which the orthonormality relation

$$\int d\Omega {}_s Y_l^{m*} {}_s Y_{l'}^{m'} = \delta_{ll'} \delta_{mm'}, \quad (24)$$

and the recursion relations of spherical Bessel functions

$$\frac{j_l(x)}{x} = \frac{1}{2l+1} [j_{l-1}(x) + j_{l+1}(x)] \quad (25)$$

have been used. Finally, the power spectrum can be obtained by substituting equation (23) into (19),

$$C_{(E,B)l} = (4\pi)^2 \frac{9}{16} \frac{(l+2)!}{(l-2)!} \sum_m \int k^2 dk \left\langle \left| \int d\tau g(\tau) X^{(m)}(\mathbf{k}, \tau) T_{(E,B)l}^{(m)}(kr) \right|^2 \right\rangle. \quad (26)$$

3. NUMERICAL RESULTS

To calculate the polarization anisotropy spectrum using the results discussed above, we use the publicly available code CMBFast (Seljak & Zaldarriaga 1996). We modify the ionization history in this code to follow the more realistic case from our previous work (Paper I), in which the reionization history of the universe is determined by a semi-analytic model of galaxy formation. In Paper I we calculated the ionizing luminosities of galaxies, including the effects of absorption by interstellar gas and dust on the escape fraction f_{esc} (the fraction of ionizing photons produced by stars that are able to escape from the galaxy in which they originated into the IGM), and follow the propagation of the ionization fronts around each galaxy. The mass in the spherical ionization front is determined by (Shapiro & Giroux 1987)

$$\frac{1}{m_{\text{H}}} \frac{dM}{dt} = S(t) - \alpha_{\text{H}}^{(2)} a^{-3} f_{\text{clump}} n_{\text{H}} \frac{M}{m_{\text{H}}}, \quad (27)$$

where n_{H} is the comoving mean number density of hydrogen atoms (total, HI and HII) in the IGM, m_{H} is the mass of a hydrogen atom, $a(t)$ is the scale factor of the universe normalized to unity at $z = 0$, t is time (related to the conformal time by $dt = d\tau/a$), $S(t)$ is the rate at which ionizing photons are being emitted and $\alpha_{\text{H}}^{(2)}$ is the case B recombination coefficient. The clumping factor $f_{\text{clump}} \equiv \langle \rho_{\text{IGM}}^2 \rangle / \bar{\rho}_{\text{IGM}}^2$ gives the effect of clumping on the recombination rate of hydrogen in the IGM. A larger f_{clump} increases the recombination rate resulting in a delay of the reionization epoch. We use $f_{\text{clump}}^{(\text{halos})}$ as defined in Paper I. Having the ionization history, at this point, we can obtain the first order power spectrum of the polarization anisotropies. In this case, we only consider the scalar mode of the primordial perturbations which are axially symmetric. Thus, we set $m = 0$ in the equation (26) and find no magnetic mode can be produced (see Table. 1). However, the second order effect is more complicated as the source term contains δ_e and $\Delta_{T_2}^{(m)}$, i.e., $m = 0, \pm 1$ and ± 2 should be considered. The time evolution of the temperature quadrupole components with different m in the \mathbf{k} -basis is obtained using equation (13), and $\Delta_{T_2}^{(0)}$ also is calculated by the modified CMBFast code. This leaves only the power spectrum of the electron density perturbation δ_e unknown, which should be calculated precisely from the distribution of ionized regions with different sizes and shapes and with a correlated spatial distribution. An exact treatment requires a high resolution simulation with physical processes such as gas dynamics and radiative transfer included and so requires large amounts of computing time. Here we obtain δ_e from Paper I in which an N-body simulation is used. The simulation volume, which is a box of length $141.3h^{-1}\text{Mpc}$ and contains 256^3 dark matter particles each of mass $1.4 \times 10^{10}h^{-1}M_{\odot}$, is divided into 256^3 cubic cells. An ionizing luminosity is put in the center of mass of any halo containing more than 10 particles. Ionizing photons which originate from lower mass halos (which are not resolved in the simulation) are added by assuming that these unresolved halos trace the remaining mass of the simulation (i.e. that mass which is not part of a resolved halo). In Paper I we demonstrated that the locations of unresolved sources do not significantly affect the resulting anisotropy spectrum. Which regions of the simulation become ionized is determined by one of five toy models. In all cases, the total mass of hydrogen ionized is assumed to be the same as for a large-scale homogeneous distribution with the specified clumping factor, calculated by use of equation (27).

Model A (Growing front model) Ionize a spherical volume around each halo with a radius equal to the ionization front radius for that halo assuming a large-scale uniform distribution of HI. Since the HI in the simulation is *not* uniformly distributed, and also because some spheres will overlap, the ionized volume will not contain the correct total mass of HI. We therefore scale the radius of each sphere by a constant factor, f , and repeat the procedure. This process is repeated, with a new value of f each time, until the correct total mass of HI has been ionized.

Model B (High density model) In this model we ignore the positions of halos in the simulation. Instead we simply rank the cells in the simulation volume by their density. We then completely ionize the gas in the densest cell. If this has not ionized enough HI we ionize the second densest cell. This process is repeated until the correct total mass of HI has been ionized.

Model C (Low density model) As model B, but we begin by ionizing the least dense cell, and work our way up to cells of greater and greater density. This model mimics that of Miralda-Escudé, Haehnelt & Rees (2000).

Model D (Random spheres model) As Model A but the spheres are placed in the simulation entirely at random rather than on the dark matter halos. By comparing to Model A this model allows us to estimate the importance of the spatial clustering of dark matter halos.

Model E (Boundary model) Ionize a spherical region around each halo with a radius equal to the ionization front radius for that halo. This may ionize too much or not enough HI depending on the density of gas around each source. We therefore begin adding or removing cells at random from the boundaries of the already ionized regions until the required mass of HI is ionized.

From the results of the simulation, we calculate δ_e as

$$\delta_e(\mathbf{x}, \tau) = \frac{x_e(\mathbf{x}, \tau)(1 + \delta)}{\bar{x}_e(\tau)} - 1, \quad (28)$$

where x_e is the ionized fraction (which we take to equal 1 in ionized regions and 0 in neutral regions) and δ is the dark matter overdensity (i.e. we assume that fluctuations in the gas density follow those in the dark matter). Here \bar{x}_e is defined as the mass-averaged ionized fraction in the IGM.

We fix the cosmological parameters to be $\Omega_0 = 0.3$, $\Lambda_0 = 0.7$, Hubble constant $H_0 = 70$ km/s/Mpc and $\sigma_8 = 0.9$. We will consider the effects of varying f_{esc} and Ω_b on the polarization anisotropies and also examine the polarization power spectrum in all five toy models for the distribution of ionized regions. We plot the visibility functions of the ionization histories in our simulation with different f_{esc} (panel (a)) and Ω_b (panel (b)) in Fig. 1. We find that the visibility function depends strongly on f_{esc} as shown in panel (a) in which $\Omega_b = 0.02$. The value of Ω_b determines the cooling rate (and so star formation rate) in our model of galaxy formation and also alters the recombination rate in the IGM, and so affects the time at which reionization occurs (panel (b)). Note that when we vary Ω_b and f_{esc} , we also vary the fraction of brown dwarfs in the IMF used in the galaxy formation model, in such a way that the model always fits the “knee” of the observed $H\alpha$ luminosity function of galaxies at $z = 0$ (see Paper I for more details). Therefore the production of ionizing photons does not simply scale with Ω_b .

In Fig. 2, we show how the primordial polarization anisotropies are distorted by free electrons at the reionization epoch using the modified CMBFast code. We find, first, the rescattering at the reionization epoch generates a new anisotropy at *large-scales* because the horizon has grown to a much larger size by reionization than it was at recombination ($z \simeq 1100$). More specifically, the location of the new peak reveals the horizon size at last scattering and its height reveals the duration of last scattering, i.e., this new peak is sensitive to the optical depth to the reionization epoch. To see how the distortion of the primordial polarization depends on the optical depth to reionization, κ_i , we plot the resulting power spectrum for various values of f_{esc} in panel (a). We find that the boost in the large-scale power depends strongly on the value of f_{esc} . (The optical

depth is 0.034, 0.017 and 0.014 for $f_{\text{esc}} = 1.0, 0.1$ and 0.05 respectively.) The location of the new peak depends on the reionization epoch which is characterized by the peak of the visibility function as shown in Fig. 1. From numerical simulations of the Boltzmann code for different reionization epochs and cosmological parameters, we obtain a fitting formula for the peak location l_{peak} as a function of the reionization epoch z_i :

$$l_{\text{peak}} = 0.74(1 + z_i)^{0.73}\Omega_0^{0.11}. \quad (29)$$

This fit is consistent with the peak locations shown in Fig. 2.

On the other hand, the polarization fluctuations are suppressed on small scales by rescattering since a fraction of the photons coming from the recombination epoch is scattered after reionization. The tiny optical depth for rescattering causes little erasure of power on small scales, but the new peak reaches an amplitude of $\sim 0.05\text{--}0.1\mu\text{K}$. From panel (b), we can see that the suppression also depends on κ_i .

Let us discuss the second order effect. In Fig. 3, we show the contribution to C_{El} and C_{Bl} from *each* value of m for Model A. For $m = 0$, only the E-mode is generated because $T_{Bl}^{(0)} = 0$ (see Table. 1). Our numerical results show that the E-mode (the B-mode) from $m = \pm 2$ ($m = \pm 1$) dominates the one from ± 1 (± 2) by more than four orders of magnitude. Moreover, the total power spectra of the E- and B-modes are almost exactly the same. The difference is less than 10^{-6} which may be caused by numerical errors. These results are consistent with previous work by Hu (2000), in which the weak-coupling approximation was employed.

In Fig. 4, we plot the second order power spectrum of the polarization in the five toy models with fixed extreme escape fraction $f_{\text{esc}} = 1$. Although the shapes of the curves are all very similar, their amplitudes are different. Note that the reduction in power above $l \sim 10000$ is artificial and due to the limited resolution of the N-body simulation we use. The power spectrum amplitude around the peak ($l \approx 10000$) varies by a factor ≈ 2.5 , depending on which of the models A–E is used. In Paper I we argued that the amplitude of the curves is affected by the strength of the correlations present in each model. As a result, the “high density” model is the most strongly correlated and has the highest amplitude, and conversely the “low density” model has the lowest amplitude.

However, the first order power spectra produced by the different models show little difference between them (no more than 10%). Thus, the second order effect should be a more powerful tool for the study of the clustering of the ionized gas and the physics of reionization. We also see that the second order signal dominates over the first order signal on small scales ($l \gtrsim 6000$). This will be useful for a high resolution experiment since we will be able to distinguish the secondary signal from the primordial one.

In Fig. 4, we also compare our results to the toy model of Gruzinov & Hu (1998), in which the reionization is determined by three free parameters. In their model, each luminous source is assumed to ionize a spherical region with fixed comoving radius R , the first source appears at

redshift z_i and reionization is complete after an interval δz . An artificial assumption that luminous sources appear at random locations in space is made, so there are no correlations between the positions of the ionized spheres. Assuming that the spheres remain ionized forever, the fractional ionization increases with increasing number density of ionized spheres during δz until the universe is completely ionized. We choose $R = 0.85h^{-1}$ Mpc, $z_i=11$ and $\delta z = 5$ to match the position of the peak in our models. For small l , little power is generated in this model since the patches are uncorrelated by design, while scales smaller than the peak of the toy model cannot be well determined from our simulation because of the limited resolution.

The amplitude of the second order polarization power spectrum also depends on the value of Ω_b which affects the visibility function in equation (23). In our simulation, Ω_b is set to be 0.02, which is lower than the current estimates based on Big Bang Nucleosynthesis which imply $\Omega_b h^2 = 0.0190 \pm 0.0018$ (Burles et al. 2000). In Fig. 5, we increase Ω_b to 0.04. If the evolution of the ionized regions were the same in both models, we could expect the amplitude to increase a factor of four (eq. 14). However, the delay of reionization resulting from this increase in Ω_b , as was shown in Fig. 1, reduces the factor to 2.8.

So far we have set $f_{\text{esc}} = 1.0$ only. Whilst this may in fact be a plausible value for high-redshift galaxies based on recent observations (Steidel Pettini & Adelberger 2000), it is instructive to examine the effects of changing f_{esc} . Using Model A we examine the effects on the second order polarization anisotropies of varying f_{esc} . The results are shown in Fig. 6. In contrast to the first order anisotropies, the amplitude of the second order anisotropies increases weakly with increasing f_{esc} , with the extreme value $f_{\text{esc}} = 1.0$ differing from the others by only a factor of about 1.6. This is because the source term for the first order polarization anisotropies is the visibility function multiplied by the temperature quadrupole, $g(\tau)\Delta_{T2}$. Since the temperature quadrupole changes slowly with time, we can say that the power spectrum is mainly determined by the visibility function. However, the source term for the second order anisotropies is the visibility function multiplied by δ_e , whose time evolution is roughly proportional to $1/(1+z)$. Thus, the signal in the secondary anisotropies is more strongly weighted to low z , where the differences between models with different f_{esc} are less significant.

4. CONCLUSIONS

We have investigated the polarization anisotropies created during the reionization epoch, in particular focusing on the second order effect. It is found that the boost in the large-scale polarization anisotropy is very sensitive to the optical depth to reionization κ_i , with larger optical depths giving larger boosts. From previous work (Paper I), the optical depth from the present to the reionization epoch, κ_i , is typically in the range 0.014 to 0.048. This causes a new peak at large scales with amplitude around $0.05 \sim 0.15\mu\text{K}$. The position of the peak is determined by the size of the horizon at reionization. If this peak can be detected by future experiments such as Planck, it would offer valuable evidence to guide our understanding of reionization of the universe.

We have also studied the second order polarization effects resulting from the coupling of fluctuations in the free electron number density, δ_e , with the quadrupole of the temperature anisotropies. Having obtained δ_e from a high resolution simulation in previous work (Paper I), we summarize the second order polarization anisotropies as follows: (1) The second order effect dominates over the first order effect on small scales ($l > 6000$). (2) The B-mode of polarization is induced as well as the E-mode. The angular power spectra of these two modes C_{El} and C_{Bl} are the same. (3) The shape of the $C_{(E,B)l}$ are very similar in all of the toy models considered for the spatial distribution of the ionized regions, but differ considerably from the toy model of Gruzinov & Hu (1998). The reason for this difference is the spatial correlations of the ionized regions in our model, which determine the shape and also the amplitude of $C_{(E,B)l}$. Though the difference in amplitude between toy models is large in the second order effect, for example, Models B and C differ by a factor of 2.5, the different models give very similar results for the first-order power spectrum. This implies that the second-order power spectrum is a more powerful tool for understanding reionization than the first order power spectrum. (4) The amplitude also depends on the value of Ω_b . If the evolution of the ionized regions were the same for any value of Ω_b , we would expect the amplitude to be proportional to Ω_b^2 . However, the scaling in our model is somewhat weaker because increasing the value of Ω_b delays reionization. In our calculation, the second-order power spectrum for an $\Omega_b = 0.04$ model has an amplitude 2.8 times greater than for an $\Omega_b = 0.02$ model. (5) The amplitude of $C_{(E,B)l}$ depends only weakly on f_{esc} (and so on the redshift of reionization). Since the amplitude of the power spectrum for the extreme value of $f_{\text{esc}} = 1.0$ differs from that with $f_{\text{esc}} = 0.1$ only by a factor of about 1.5, the results in Fig. 4 and Fig. 5 should be mostly independent of the true value of f_{esc} .

While second order effects can make a significant contribution to the temperature anisotropy ($\sim 0.1\text{--}1\mu\text{K}$), the second-order polarization anisotropies generated by inhomogeneous reionization are, as expected, very small. We conclude that the signals are typically of order several nK, comparable to estimates from other authors studying Vishniac-type polarization (Seshadri & Subramanian 1998) or toy models of patchy reionization (Weller 1999). A signal of this amplitude is below the detectability limits of the Planck Surveyor mission. However, it provides more information about galaxy formation and the process of reionization than the first order effect. Therefore, detection of this signal should be a key aim of a post-Planck experiment with increased sensitivity and resolution in the next decade.

We thank U. Seljak and M. Zaldarriaga for the use of CMBFast, the Virgo Consortium for making available the GIF N-body simulations used here, and Shaun Cole, Carlos Frenk and Carlton Baugh for allowing us to use their model of galaxy formation. GCL thanks N. Seto for useful discussion and acknowledges the fellowship of Interchange Association. NS, AN and CGL acknowledge kind hospitality of Carlos Frenk and the physics department of University of Durham during the TMR network meeting. NS is supported by the Sumitomo foundation. CGL acknowledges support at SISSA from COFIN funds from MURST and from ASI. AN and AJB acknowledge the support of the EC RTN network “The Physics of the Intergalactic Medium”.

REFERENCES

- Benson, A.J., Nusser, A., Sugiyama, N. & Lacey, C. G., 2001 MNRAS, 320, 153 (Paper I)
- Bond, J. R & Efstathiou, G., 1984, ApJ, 285, L45
- Bond, J. R. & Efstathiou, G., 1987, Mon. Not. R. Astr. Soc., 226, 655
- Bruscoli, M., Ferrara, A., Fabbri, R., & Ciardi, B., 2000, Mon. Not. R. Astr. Soc. in press
- Burles, S., Nollett, K. M. and Turner, M. S., ApJ, submitted
- Gnedin, N. Y., 2000, ApJ, **535**, 530
- Gnedin, N. Y. & Jaffe, A. H., 2000, ApJ in press (astro-ph/0008469)
- Gruzinov, A. & Hu, W., 1998, ApJ, 508, 435
- Hu, W., 2000, ApJ, 529, 12
- Hu, W., & White, M., 1997, New Astronomy, 2, 323
- Jaffe, A. H., & Kamionkowski, M., 1998, Phys. Rev. D, 58, 043001
- Kaiser, N., 1984, ApJ, 282, 374
- Ma, C-P & Bertschinger, E., 1995, ApJ, 455, 7
- Miralda-Escudé J., Haehnelt M., Rees M. J., 2000, ApJ, 530, 1
- Newman, E. & Penrose, R., 1966, J. Math. Phys., 7, 863
- Ng, K.-W. & G.-C. Liu, 1999, Int. J. Mod. Phys. D8 61-83
- Ng, K. L. & Ng, K.-W., 1996, ApJ, 456, 413
- Peebles, P. J. E. & Yu, J. T., 1970, ApJ, 162, 815
- Rees, M. J., 1968, ApJ, 153, L1
- Sakurai, J. J., *Modern Quantum Mechanics* (Addison-Wesley, New York, 1985)
- Sato, H., 1994, Prog. Theor. Phys. **92**, 34
- Shapiro, P. R., & Giroux, M. L., 1987, ApJ, 321, L107
- Seljak, U. & Zaldarriaga, M., 1996, ApJ, 469, 437
- Seshadri, T. R & Subramanian, K., 1998, Phys. Rev. D, 58, 063002
- Smoot, G. F., et al., 1992, ApJ, 369, L1

Springel, V., White, M. & Hernquist, L., 2000, submitted to ApJL (astro-ph/0008133)

Steidel, C. C., Pettini, M. & Adelberger, K. L., 2000, astro-ph/0008283

Sunyaev, R.A. & Zel'dovich, Ya. B. 1980, MNRAS, 190, 413

Weller, J., 1999, ApJ, 527, L1

Zaldarriaga, M. & Seljak, U., 1997, Phys. Rev. D 55, 1830

Zaldarriaga, M., 1997, Phys. Rev. D, 55, 1822

Valageas, P., Balbi, A. & Silk, J., 2000, submitted to A&A (astro-ph/0009040)

Vishniac, E. T., 1987, ApJ, 322, 597

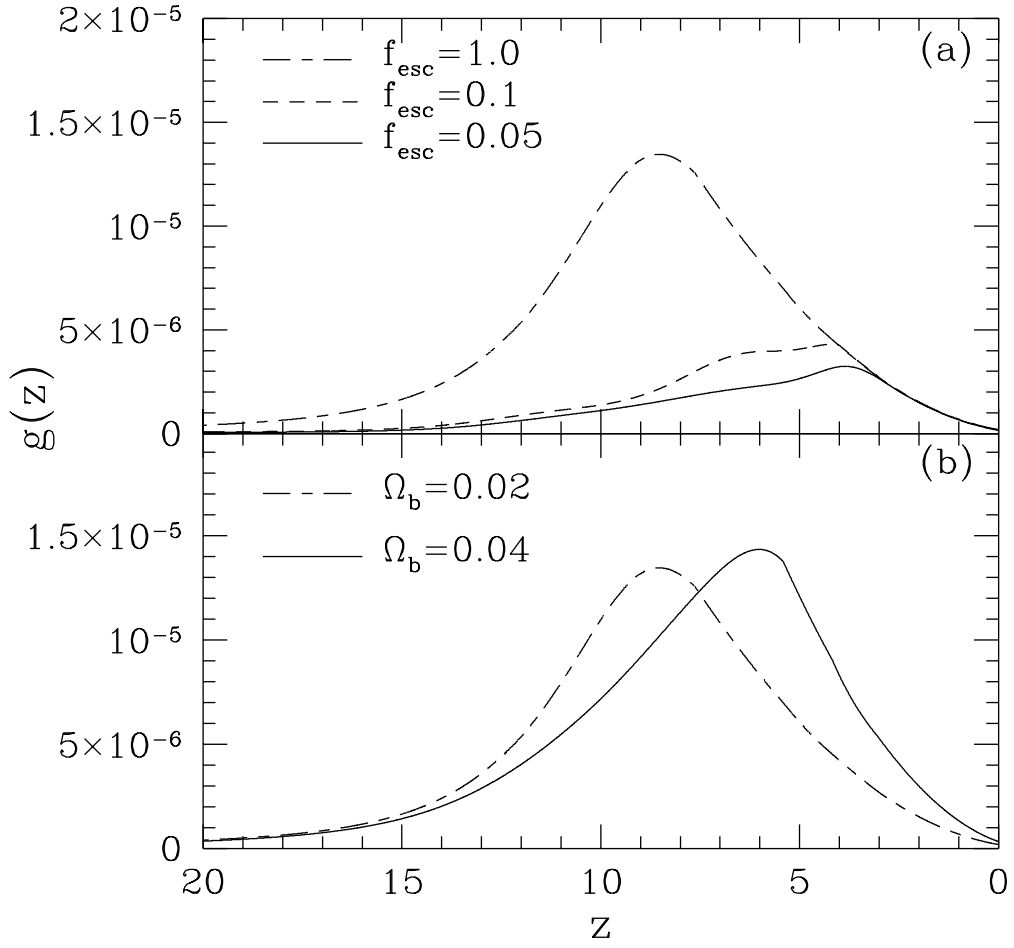


Fig. 1.— Visibility function for various escape fractions, f_{esc} , (a) and Ω_b (b) in Λ CDM models with $\Omega_0 = 0.3$, $h = 0.7$ and $\Lambda = 0.7$ in which we have used Model A for the distribution of ionized regions. The value of Ω_b in panel (a) is set to 0.02, and an escape fraction of $f_{\text{esc}} = 1.0$ is used in panel (b).

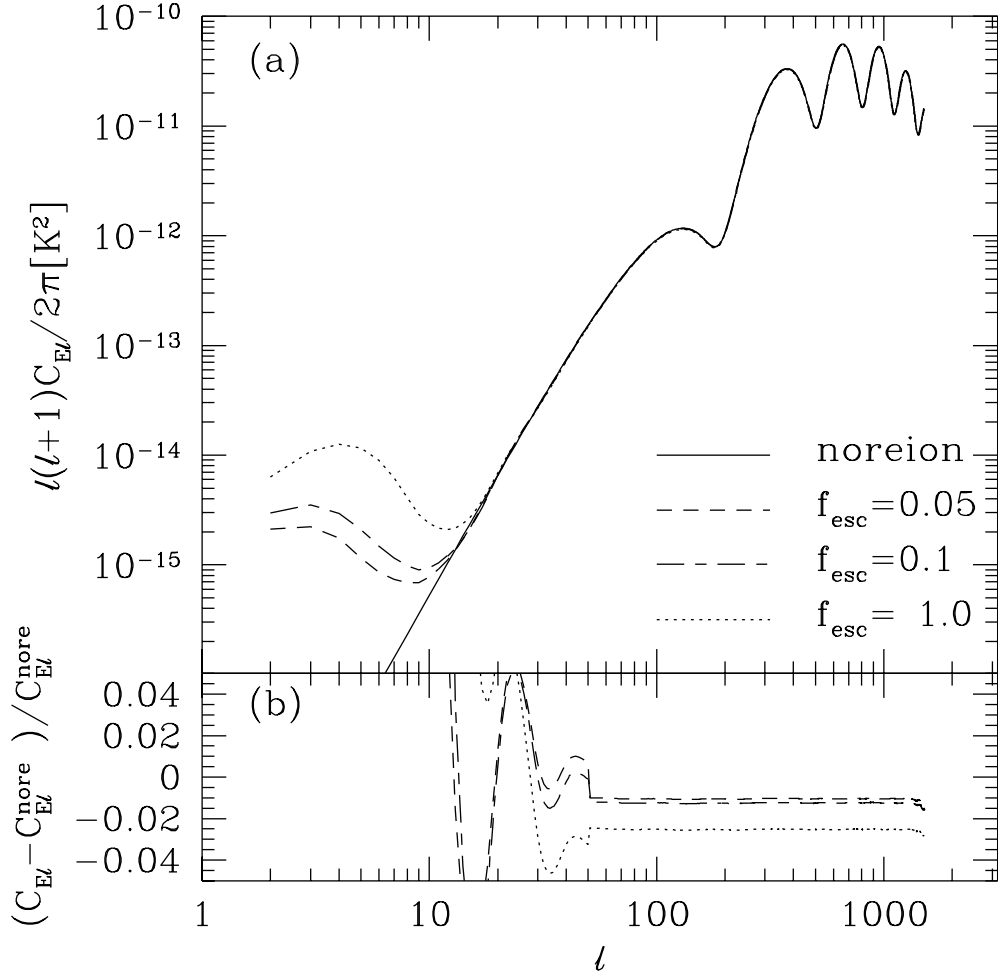


Fig. 2.— The modification of the first order polarization by reionization. (a) The angular power spectrum of the polarization for each reionization history. (B) The ratios of these to the model with no reionization. The boost on large scales and supression on small scales are due to reionization. The values of $f_{\text{esc}} = 0.05, 0.1$ and 1.0 correspond to an optical depth to reionization of $\kappa_i = 0.014, 0.017$ and 0.034 , respectively. In panel (a), the power spectrum is multiplied by the square of CMB temperature $T_{\text{CMB}} = (2.726K)^2$.

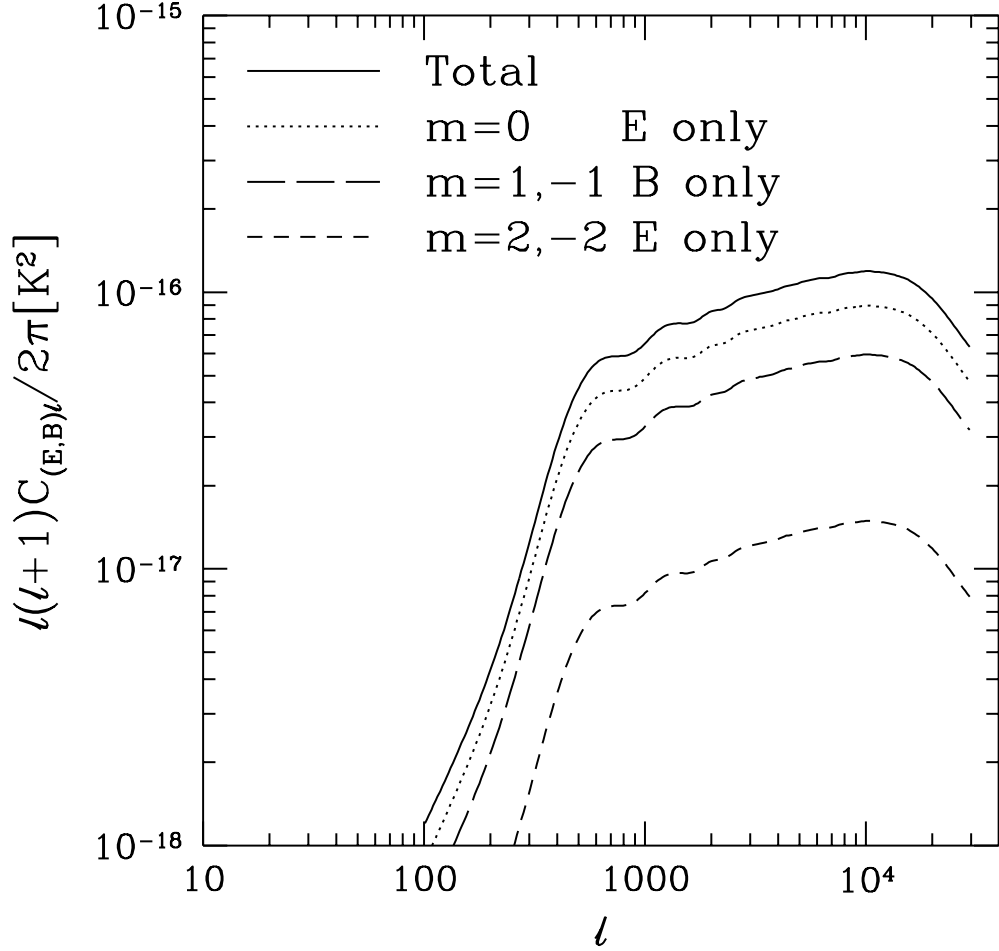


Fig. 3.— Contributions to the power spectrum of the second order effect from different values of m . The curves shown are computed using Model A with $f_{\text{esc}} = 1$. Note that the long-dashed curve shows the contribution to the B-mode from only $m = 1$ or $m = -1$ (not the sum of $m = 1$ and $m = -1$), and similarly the short-dashed curve shows the contribution to the E-mode from only $m = 2$ or $m = -2$. We find that the dominant contribution to the E-mode is from $m = 0$ and $m = \pm 2$, while for the B-mode it is from $m = \pm 1$. There is no B-mode for $m = 0$ and very small E- and B-modes for $m = \pm 1$ and $m = \pm 2$, respectively. The total power spectrum of the E-mode, plotted as the solid curve, and calculated by summing the $m = 0, \pm 1$ and ± 2 contributions, is the same as the total power spectrum of the B-mode. The power spectra are multiplied by $T_{\text{CMB}} = (2.726K)^2$.

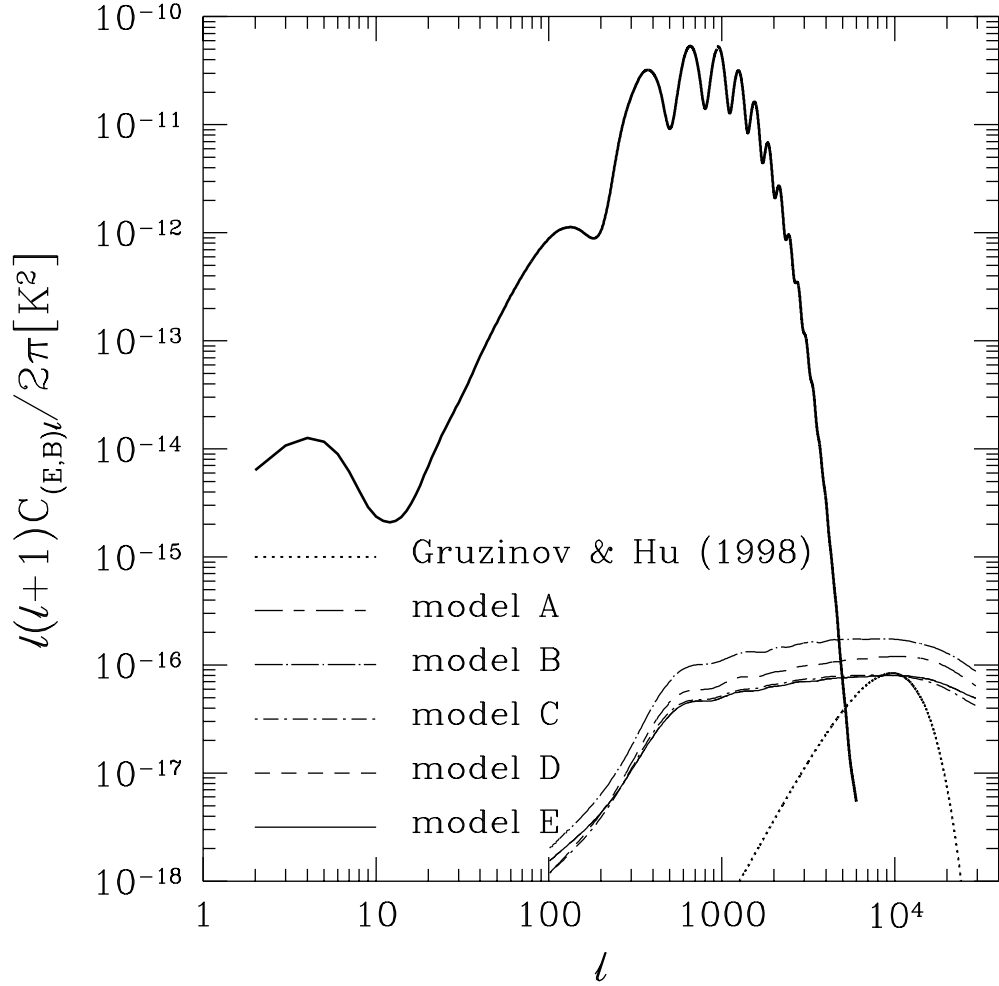


Fig. 4.— Power spectra of the second order effect for our models. For comparison, the toy model of Gruzinov & Hu (1998), in which the ionized regions are randomly distributed, is also shown. The heavy solid line shows the first-order anisotropy for $\Omega_b = 0.02$ and $f_{\text{esc}} = 1.0$. Note that only C_{El} contributes to the first-order effect, while in the second-order effect C_{El} and C_{Bl} are equal.

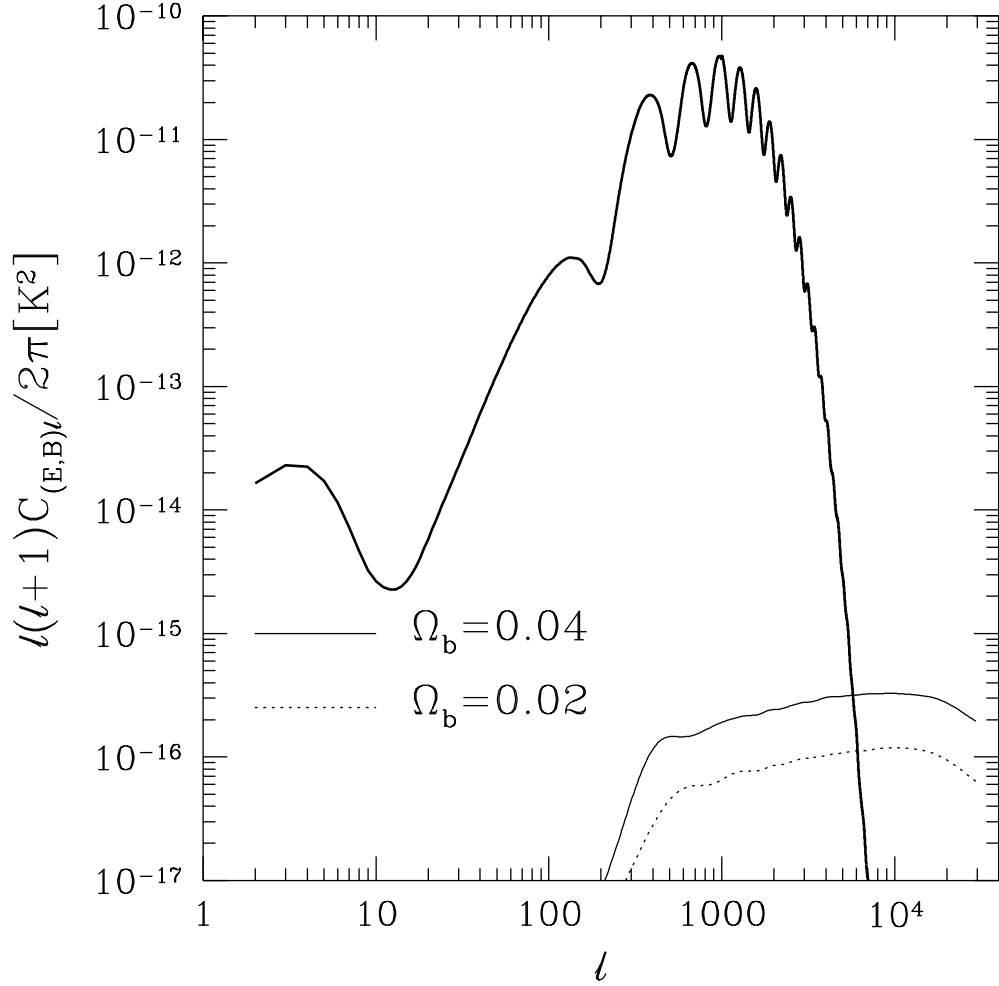


Fig. 5.— Effect on the secondary CMB polarization anisotropy spectrum of varying Ω_b . The curves shown are all computed using Model A. The solid line shows $\Omega_b = 0.04$ while the dotted line shows $\Omega_b = 0.02$. The heavy solid line shows the primary anisotropy for the model $\Omega_b = 0.04$ and $f_{\text{esc}} = 1.0$. The power spectrum is multiplied by $T_{\text{CMB}} = (2.726\text{K})^2$.

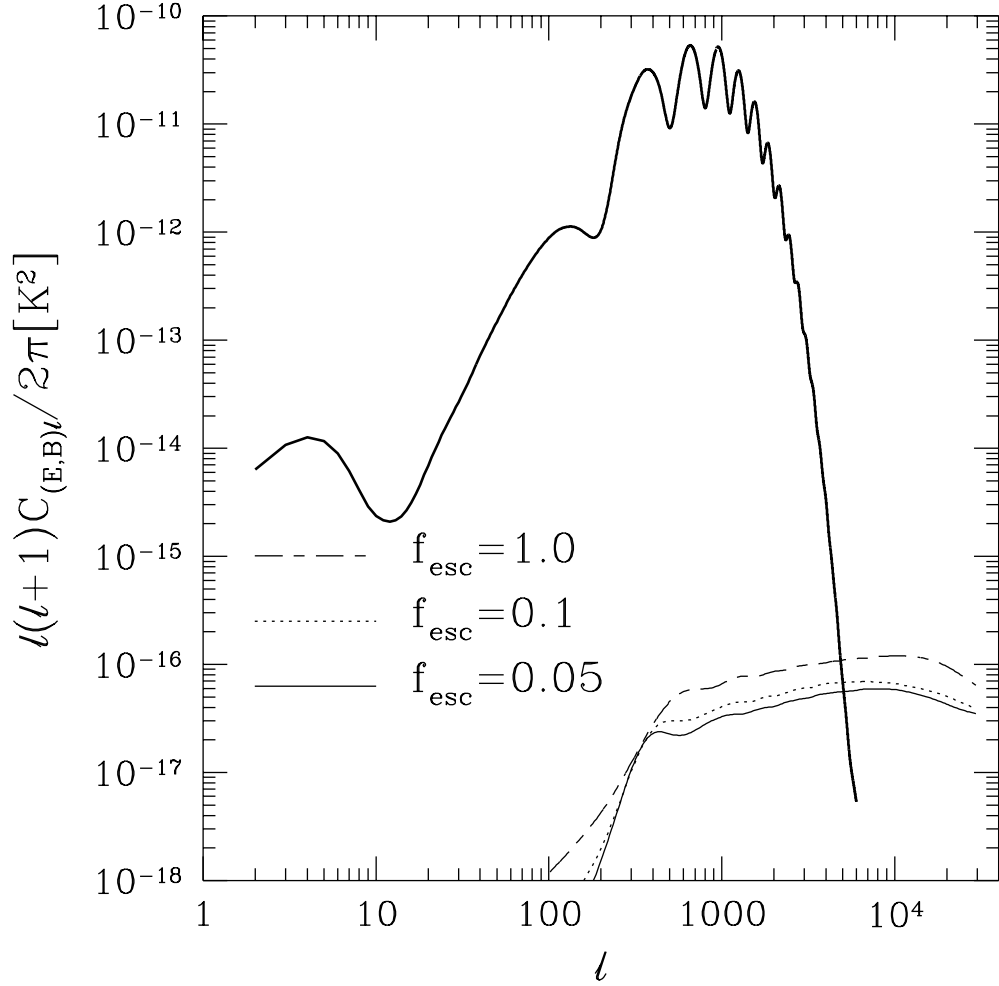


Fig. 6.— Effect on the secondary CMB polarization anisotropy spectrum of varying the escape fraction f_{esc} . The curves shown are all computed using Model A and $\Omega_b = 0.02$. Escape fractions of 1.0, 0.1 and 0.05 are shown as indicated in the figure. The heavy solid line shows the primary anisotropy for the model $\Omega_b = 0.02$. The power spectrum is multiplied by $T_{\text{CMB}} = (2.726\text{K})^2$.